Optimizing cone beam CT scatter estimation in egs_cbct for a clinical and virtual chest phantom

Slot Thing, Rune; Mainegra-Hing, Ernesto

Published in:
Medical Physics

DOI:
10.1118/1.4881142

Publication date:
2014

Medical Physics
The International Journal of Medical Physics Research and Practice

Optimizing cone beam CT scatter estimation in egs_cbct for a clinical and virtual chest phantom

Rune Slot Thing and Ernesto Mainegra-Hing

Citation: Medical Physics **41**, 071902 (2014); doi: 10.1118/1.4881142
View online: http://dx.doi.org/10.1118/1.4881142
View Table of Contents: http://scitation.aip.org/content/aapm/journal/medphys/41/7?ver=pdfcov
Published by the American Association of Physicists in Medicine

Optimizing cone beam CT scatter estimation in egs_cbct for a clinical and virtual chest phantom

Rune Slot Thing[a)]
Institute of Clinical Research, University of Southern Denmark, Odense 5000, Denmark and Laboratory of Radiation Physics, Odense University Hospital, Odense 5000, Denmark

Ernesto Mainegra-Hing[b)]
Ionizing Radiation Standards, National Research Council of Canada, Ottawa K1A 0R6, Canada

(Received 18 December 2013; revised 25 April 2014; accepted for publication 11 May 2014; published 9 June 2014)

Purpose: Cone beam computed tomography (CBCT) image quality suffers from contamination from scattered photons in the projection images. Monte Carlo simulations are a powerful tool to investigate the properties of scattered photons. egs_cbct, a recent EGSnrc user code, provides the ability of performing fast scatter calculations in CBCT projection images. This paper investigates how optimization of user inputs can provide the most efficient scatter calculations.
Methods: Two simulation geometries with two different x-ray sources were simulated, while the user input parameters for the efficiency improving techniques (EITs) implemented in egs_cbct were varied. Simulation efficiencies were compared to analog simulations performed without using any EITs. Resulting scatter distributions were confirmed unbiased against the analog simulations.
Results: The optimal EIT parameter selection depends on the simulation geometry and x-ray source. Forced detection improved the scatter calculation efficiency by 80%. Delta transport improved calculation efficiency by a further 34%, while particle splitting combined with Russian roulette improved the efficiency by a factor of 45 or more. Combining these variance reduction techniques with a built-in denoising algorithm, efficiency improvements of 4 orders of magnitude were achieved.
Conclusions: Using the built-in EITs in egs_cbct can improve scatter calculation efficiencies by more than 4 orders of magnitude. To achieve this, the user must optimize the input parameters to the specific simulation geometry. Realizing the full potential of the denoising algorithm requires keeping the statistical uncertainty below a threshold value above which the efficiency drops exponentially.
 [http://dx.doi.org/10.1118/1.4881142]

Key words: Monte Carlo, EGSnrc, CBCT imaging, image quality, x-ray scatter, variance reduction techniques

1. INTRODUCTION

In-room imaging is an integral part of modern image-guided radiotherapy (IGRT). Kilovoltage (kV) cone beam computed tomography (CBCT) is the modality of choice for many clinics offering IGRT, since it provides high contrast images of the patient in the treatment position.

With the increasing number of CBCT devices in use worldwide, the focus on CBCT image quality is increasing too. It is well established that the image quality of CBCT is inferior to CT imaging, and that the main reason for the difference is the larger contamination from scattered photons in CBCT.[1] The nature of scattered photons in CBCT imaging has been studied extensively, and the most accurate method to perform such studies is through the use of Monte Carlo (MC) simulations.[1–4]

The main limitation of MC calculations has been the potentially very long calculation times (see, e.g., Ref. 1). This has lead to the development of a new EGSnrc (Refs. 5 and 6) user code called egs_cbct,[7,8] designed to provide efficient CBCT scatter calculations through the use of several variance reduction techniques (VRTs) combined with a denoising algorithm. egs_cbct was released with EGSnrc V4 2.4.0 in March 2013, and has already been used for a few studies.[9–12]

In one of the original papers describing egs_cbct, the use of VRTs was reported to improve the scatter calculation efficiency by 3 orders of magnitude for a chest phantom.[8] However, this paper did not highlight the need for geometry specific optimization of the VRT parameters, or how such optimization should be performed.

The present paper provides guidelines on how to take advantage of the powerful efficiency improving techniques (EITs) in egs_cbct. Two distinct geometries are simulated, each with two different x-ray sources. The efficiency increase and optimization related to each of the available EITs is discussed, and the method described can be applied to any MC simulation carried out with egs_cbct.

2. MATERIALS AND METHODS

MC calculations were performed with egs_cbct,[7,8] an EGSnrc (Refs. 5 and 6) user code for CBCT related calculations. The XCOM photon cross section compilation[13] was used, and coherent (Rayleigh) scattering and incoherent (Compton) scattering with binding corrections were turned on. The low-energy photon transport cut-off, PCUT, was set to 1 keV. No electrons are transported in egs_cbct by selecting a very high low-energy electron transport cut-off, ECUT.

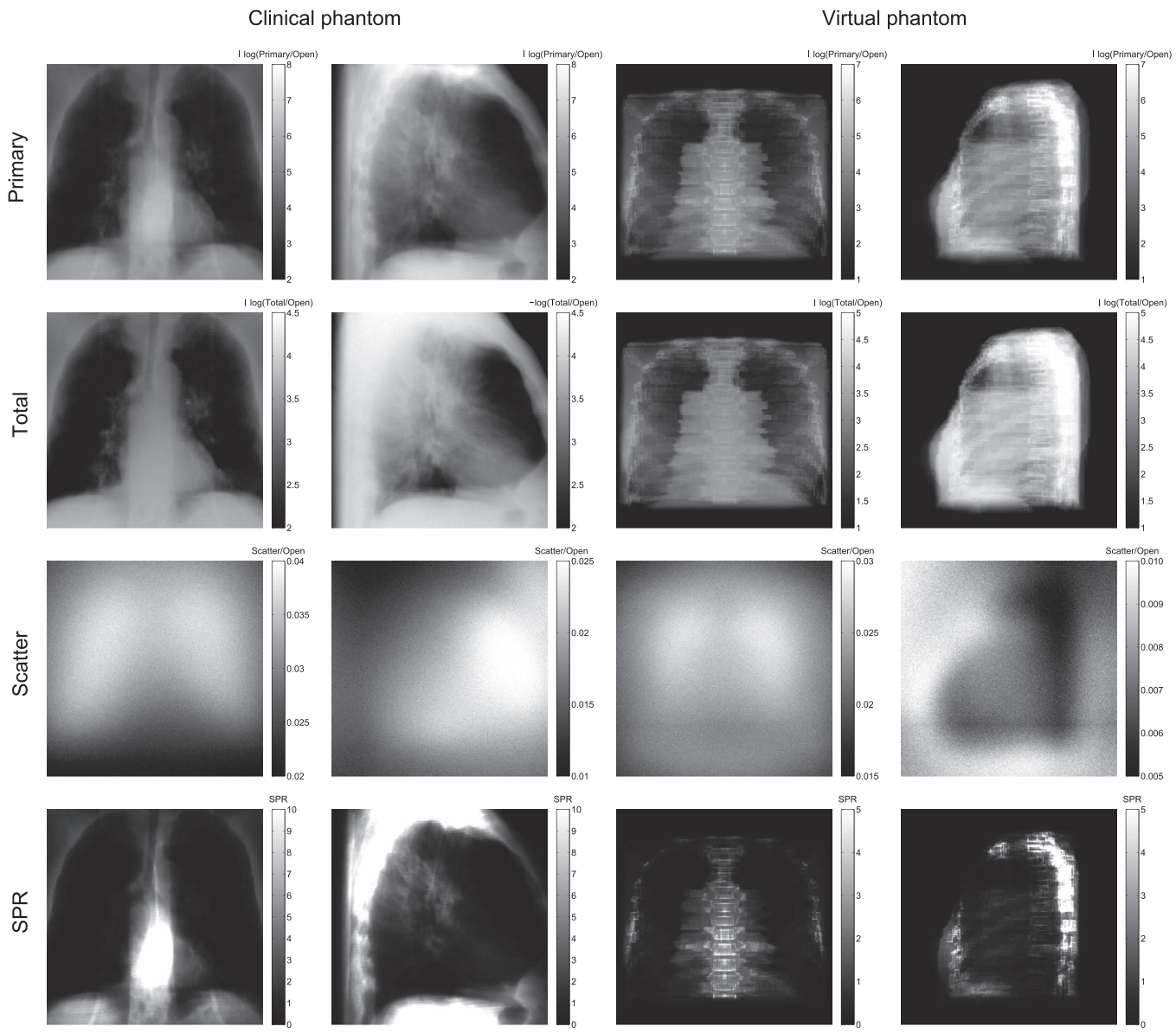

FIG. 1. Anterior–posterior and lateral views of the clinical and virtual phantoms. Primary and total images have been normalized to the open signal and log transformed, while the scatter images have only been normalized to the open signal. Scatter-to-primary-ratio (SPR) values of more than 40 were found in the lateral clinical image. Images were produced with the 60 keV source for both phantoms.

2.A. Simulation geometry

The main simulation geometry in the present investigation was modeled after an Elekta XVI CBCT unit (Elekta Ltd., Crawley, West Sussex, UK). This unit has a source-to-axis-distance (SAD) of 100 cm and a source-to-detector-distance (SDD) of 153.6 cm. The detector is made of 512 × 512 pixels with a pitch of 0.8 mm. Detector signal was calculated as air kerma.

A 512 × 512 × 100 patient phantom with voxel size 1 × 1 × 3 mm was created from a CT scan of a lung cancer patient previously treated at Odense University Hospital. CT numbers were converted to densities using a piecewise linear ramp, and the patient was modeled as made of water with varying density. The MC model of the XVI unit and the patient phantom will be referred to as the *clinical case*. Anterior–posterior and lateral projection images of the clinical phantom are shown in Fig. 1.

To investigate the effects of geometry and CBCT setup on the efficiency, simulations were also performed for a 200 × 200 × 200 chest phantom taken from the voxelized human phantom FAX06.[14] This phantom was placed at a SAD of 100 cm and signal was estimated on a 512 × 512 flat panel detector at a SDD of 155 cm. Phantom voxel size was 1.5 × 1.2 × 1.2 mm and the detector pitch was 0.9 mm. This setup will be called the *virtual phantom case*. Two projection images of the virtual phantom are shown in Fig. 1.

Most simulations were performed using a 60 keV uniform photon point source. Downes *et al.* reported the mean energy of the XVI x-ray unit to be 61.2 keV,[15] and the source energy was chosen according to this finding. Simulations with a 120 kV source were also included to assess the impact on the

efficiency when sampling photons from an energy spectrum. The spectrum was taken from a previous MC simulation of the Comet MXR-320 x-ray tube used at the National Research Council of Canada for routine calibrations.[16]

2.B. Efficiency improving techniques

Several EITs are implemented in egs_cbct. Except for the locally adaptive denoising algorithm, these are all true VRTs described extensively in a previous publication,[8] to which the reader is referred for details. For completeness, a short description of each EIT is included below.

All simulations were compared to a lengthy baseline simulation produced without using any of the EITs. To investigate if the EITs introduced a bias in the result, the mean relative error (MRE) was calculated

$$\mathrm{MRE} = \frac{1}{N}\sum_{i=1}^{N}\frac{x_i - x_i^0}{x_i^0}. \tag{1}$$

Here, N is the number of detector pixels, x_i is the signal in pixel i from the calculation using EITs, and x_i^0 is the signal in pixel i from the baseline calculation. The result was considered unbiased if the MRE was smaller than the statistical uncertainty of the result.

Simulation efficiency ε was calculated using the expression

$$\varepsilon = \frac{1}{\mathrm{rRMSE}^2 \cdot T_{\mathrm{CPU}}}, \tag{2}$$

where rRMSE is the relative root mean square error of the scatter signal and T_{CPU} is the CPU time of the calculation. rRMSE is defined here as

$$\mathrm{rRMSE} = \left(\frac{1}{N}\sum_{i=1}^{N}\frac{\Delta x_i{}^2}{x_i{}^2}\right)^{\frac{1}{2}}, \tag{3}$$

where x_i and Δx_i are the value of the signal and its estimated statistical uncertainty in pixel i, respectively. N is the number of pixels with nonzero signal.

Only a single projection image (anterior–posterior) was simulated and used to optimize the EIT parameters. As shown by Mainegra-Hing and Kawrakow,[8] the scatter calculation efficiency varies with the projection angle. However, this variation is similar for all EITs.

To determine the scatter calculation efficiency, only short simulations are required. It must however be noted that large statistical uncertainties in the scatter distributions can introduce fluctuations in the efficiency calculations. Thus, statistical uncertainties of less than 10% were desired in the present study when determining the calculation efficiency.

2.B.1. Forced detection

To improve the scoring efficiency in egs_cbct, the contribution to the detector is scored for all photons aimed at the detector before they are transported, rather than when each photon crosses the detector. An exact ray-tracing algorithm is implemented to account for the attenuation through the phantom.

2.B.2. Path length transformation

The major contribution to the detector signal from scattered photons arises from photons scattered near the exit side of the geometry.[8] To increase the sampling of scatter events in this region of the geometry, a path length stretching technique is implemented in egs_cbct. This technique does not exhibit a dependency on the particle's direction as is the case of the well-known exponential transformation of the photon path length. The probability distribution $p(\eta)$ for selecting the number of mean free paths η is modified by an appropriate transformation to be

$$p(\eta) = \frac{2\cdot\eta_0{}^2}{(\eta+\eta_0)^3}, \tag{4}$$

with η_0 an adjustable parameter (MFPTR in egs_cbct). The statistical weight must be accordingly adjusted to avoid introducing a bias in the estimation. The effect of varying η_0 on the scatter estimation efficiency was studied.

2.B.3. Delta transport

Photons not aimed at the detector are transported using so-called delta transport or Woodcock tracing. Here, the most attenuating medium in the geometry is specified by the user, providing the maximum interaction cross section $\sigma_{\max}$, and photons not aimed at the detector are transported directly to the next interaction in this medium. A fictitious interaction is selected with probability $1-\sigma/\sigma_{\max}$, where σ is the total cross section of the actual medium. This technique removes the need for boundary checks during transport away from the detector, and the contribution to the detector signal from these photons is likely to be small.

2.B.4. Denoising algorithm

A two-dimensional version of the denoising algorithm by Kawrakow[17] is implemented in egs_cbct. The denoising algorithm relies on a Savitzky-Golay filter with adaptive window size to preserve structures found in the MC calculated signal. To optimize efficiency, the algorithm first searches for the maximum acceptable denoising window size in one dimension, before searching for the maximum acceptable t window size in two dimensions.

In egs_cbct, the denoising algorithm takes three user inputs:

- **nmax:** is the maximum allowed window size in one dimension.
- **nmax2d:** is the maximum allowed window size in two dimensions (should be smaller than nmax).
- **chi2max:** is the threshold for the χ^2-test performed by the denoising algorithm to determine whether a pixel

TABLE I. Detailed information for the baseline and several simulations using different EITs. Statistical uncertainty (σ), efficiency estimates (ε and ε_{rel}), and mean relative error (MRE) is shown for the scatter signal. FS was used only in combination with forced detection (FD) and delta transport. For the FS simulations, $N_p = 9000$ was used in all cases, with $N_s = 10\,000$ in the clinical case and 2000 in the virtual case. MRE was not estimated for the virtual phantom.

Phantom	EIT	N_{Hist}	T_{CPU} (h)	σ (%)	ϵ	ε_{rel}	MRE (%)
Clinical	Baseline	1.0×10^{10}	400	4.4	3.6×10^{-4}	1.0	0.0
60 keV	FD	1.0×10^{10}	600	2.7	6.5×10^{-4}	1.8	7.3×10^{-2}
	FD + MFPTR = 5	1.0×10^{9}	56	10	5.0×10^{-4}	1.4	2.0
	FD + delta transport	1.0×10^{9}	45	8.4	8.7×10^{-4}	2.4	0.72
	FS	1.1×10^{6}	20	3.0	1.6×10^{-2}	44	7.7×10^{-2}
	FS + denoising	1.1×10^{6}	20	0.16	5.8	1.6×10^{4}	-1.6×10^{-3}
Clinical	Baseline	1.0×10^{9}	380	4.7	3.4×10^{-4}	1.0	0.0
120 kV	FS	1.1×10^{6}	19	3.1	1.5×10^{-2}	43	0.38
	FS + denoising	1.1×10^{6}	19	0.16	5.4	1.6×10^{4}	0.29
Virtual	Baseline	4.0×10^{9}	30	5.7	2.9×10^{-3}	1.0	
60 keV	FS + MFPTR = 4	1.0×10^{6}	1.7	3.0	1.8×10^{-1}	57	
	FS + MFPTR + denoising	1.0×10^{6}	1.7	0.16	58	2.0×10^{4}	
Virtual	Baseline	4.4×10^{9}	29	5.7	3.0×10^{-3}	1.0	
120 kV	FS + MFPTR = 4	1.0×10^{7}	16	1.0	1.7×10^{-1}	57	
	FS + MFPTR + denoising	1.0×10^{7}	16	7.3×10^{-2}	56	1.8×10^{4}	

value can be filtered by the algorithm or not in order to preserve potential structure.

The effect of varying all three user inputs were studied, with the constraint that nmax > nmax2d as pointed out by Kawrakow.[17]

2.B.5. Splitting + Russian Roulette

In egs_cbct, three variations of the VRT class known as splitting + RR are implemented. Only the technique referred to as fixed splitting (FS) was studied extensively in this work. FS takes two user inputs known as the primary and secondary splitting numbers, N_p and N_s. Each time a scatter event is about to occur, a primary photon will be split N_p times, and the scatter event is sampled accordingly. Statistical weights are reduced by a factor of N_p. Scattered photons not aimed at the detector are subject to a game of Russian Roulette, with a survival probability of $1/N_s$. If a scattered photon survives, any subsequent scatter event will be split by a factor of N_s to keep the statistical weights of scattered photons constant at the detector.

Two additional splitting + RR techniques known as position dependent importance sampling (PDIS) and region dependent importance sampling (RDIS) are implemented in egs_cbct, but these should be considered experimental and are only mentioned for completeness in the present study.

2.C. Hardware

Simulations were performed on the computer cluster at the Ionizing Radiation Standards group of the National Research Council of Canada. The cluster consists of 132 2.93 GHz Intel® Xeon® X5670 cores and 264 3.16 GHz Intel® Xeon® X5460 cores. Results reported here for the virtual case were obtained using the faster X5670 cores and for the clinical case using the X5460 cores. All simulation times are expressed as CPU time.

3. RESULTS

The baseline scans were performed using no less than 4 $\times$ 10^9 histories for both the clinical and virtual phantoms. Calculation times were around 400 h for the clinical phantom and 30 h for the virtual phantom, using the 60 keV and 120 kV sources (Table I). As mentioned in Sec. 2.B, only the anterior–posterior projection was simulated and used to optimize the EIT parameters. Histograms showing the error distributions of EIT-based scans from the clinical phantom compared to the baseline are shown in Fig. 2.

3.A. Forced detection

For the 60 keV clinical case, turning on forced detection increased the efficiency by 80% compared to the analog simulation. No bias was observed, and it is recommended that forced detection is used for all simulations with egs_cbct. It is further noted that MFPTR and delta transport are implemented in egs_cbct only when using forced detection, and that all splitting + RR techniques require delta transport to be turned on. Therefore, all the following results were obtained using forced detection.

3.B. MFPTR

For the 60 keV clinical case, an efficiency decrease of at least 5% was observed when using MFPTR compared to using forced detection alone. A similar efficiency decrease was found when using the 120 kV source, regardless of the MFPTR parameter used. In the virtual phantom case, efficiency improvements of 2% and 4% were found for the 60 keV and 120 kV sources, respectively. A previous study

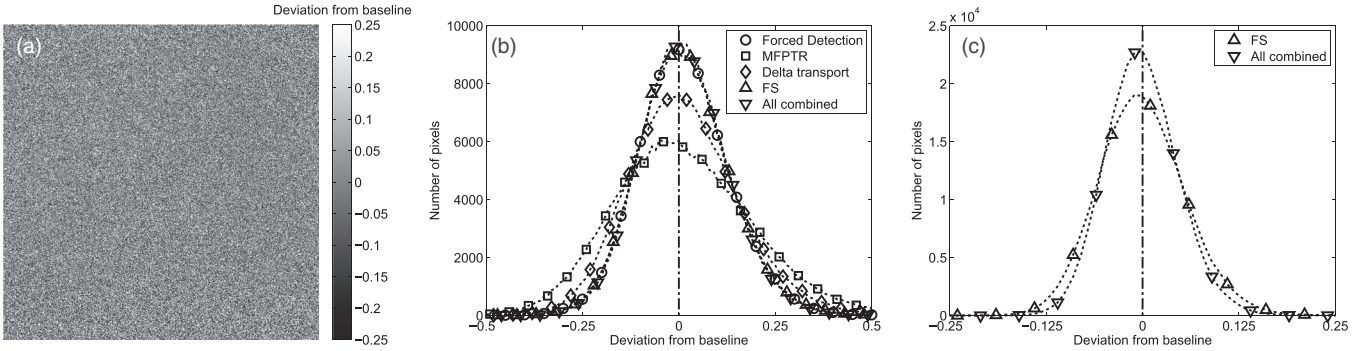

FIG. 2. Example image of the relative error between an EIT based scan using forced detection, delta transport, FS and denoising and the baseline scan for the 60 keV clinical phantom (a). All EIT parameters were optimized to produce the efficient scan. (b) and (c) show histograms of the relative error distribution for various EIT configurations described in the text (all using optimal parameters). (b) shows the investigated EITs for the clinical phantom and the 60 keV source, and (c) the EITs for the 120 kV spectrum and the clinical phantom.

showed the efficiency to increase by 24% when using MFPTR,[8] and these differences underline the importance of doing VRT optimization specific to each simulation geometry that one wishes to use.

3.C. Delta transport

Changing the delta transport medium had no effect on the efficiency in the clinical case using the 60 keV x-ray source when using lung tissue, water or bone. However, when using lung tissue, a bias of −10% was found. No bias was found when using water and bone with the clinical phantom made from water with varying density. This underlines that the delta transport medium must always be chosen as the medium with the largest mass attenuation coefficient found in the simulation geometry for this technique to be a proper VRT. This choice ensures that no bias is introduced, and does not have any efficiency penalty compared to using less attenuating media. The efficiency gain when using delta transport was 34% for the clinical case with the 60 keV source compared to using forced detection alone.

3.D. Denoising algorithm

The denoising algorithm was found to cause dramatic improvements in efficiency for all simulations. However, since the denoising algorithm is not a true VRT, it is important to ensure that it does not introduce a bias in the simulation results.

For the 60 keV virtual phantom case, varying chi2max did not introduce a bias in the results. However, when increasing the window size of the denoising algorithm (both nmax and nmax2d), the MRE was found to increase. The denoising algorithm was found most efficient when the uncertainty of the scatter distribution before denoising was less than 30%, as shown in Fig. 3.

The present investigation found that nmax = 10, nmax2d = 6, and chi2max = 20 produced the most efficient calculations without introducing a bias for the virtual phantom case. For higher numbers of chi2max, the efficiency did not increase further. Increasing the value of nmax and nmax2d did increase the efficiency, but at the cost of an increased MRE. Relative to the analog simulation, the efficiency improved by a factor of 360 with the recommended parameters.

3.E. Splitting + RR techniques

Of the three implemented splitting + RR techniques in egs_cbct, the conceptually simple FS technique was found to be as efficient as the more complex PDIS and RDIS techniques when combined with the denoising algorithm. For all three splitting techniques, the primary splitting number, or splitting factor, was found to be the most important parameter to optimize. All three splitting techniques also require the user to specify a secondary splitting number N_s, to which the efficiency was found to have little sensitivity.

3.E.1. FS

For the FS technique, the relative efficiency as a function of the primary splitting number N_p is plotted in Fig. 4. The highest efficiency was found at $N_s = 10\,000$ and with N_p between 3000 and 9000 in the clinical case for both

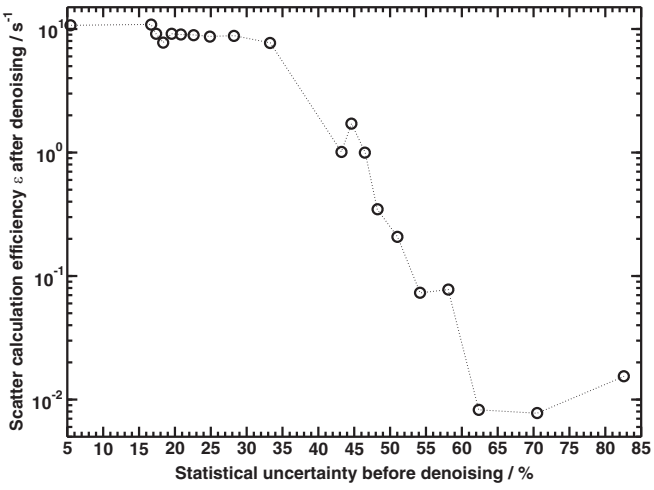

FIG. 3. Dependency of the denoising algorithm performance on the statistical uncertainty of the simulation result prior to denoising for the 60 keV virtual phantom case for nmax = 10, nmax2d = 6, and chi2max = 20.

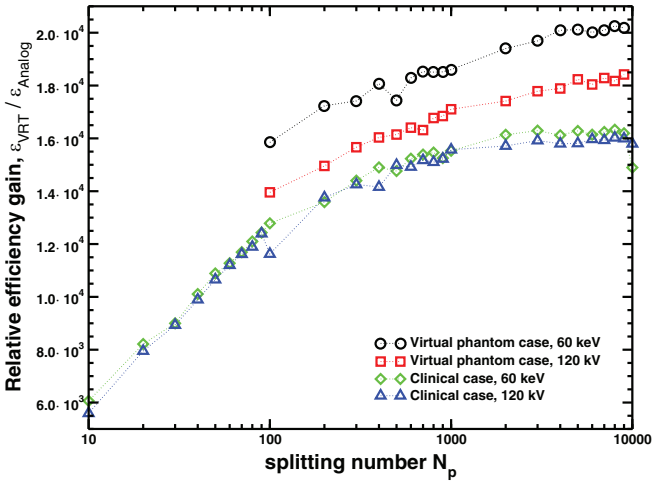

FIG. 4. Relative scatter calculation efficiency increase as a function of the splitting number N_p using the FS splitting technique combined with forced detection, delta transport, and denoising.

sources. Combined with the denoising algorithm, delta transport and forced detection, the efficiency increased by a factor of 16 000 compared to the baseline scan. Without denoising, the efficiency increase in the clinical case was a factor of 45.

Similarly, the optimum FS parameters in the virtual phantom case were $N_s = 2000$ and N_p between 4000 and 9000 for both sources. The efficiency gain compared to an analog calculation was about 20 000 for the monoenergetic source and 18 000 for the 120 kV spectrum when combined with the denoising algorithm. When no denoising was used, this gain was reduced to 58 and 56 times, respectively.

3.E.2. PDIS *and* RDIS

The more sophisticated PDIS and RDIS splitting techniques increased the efficiency by up to a factor of 2 compared to FS in the virtual phantom case when no denoising was used. However, they were only found as efficient as FS in the clinical case and in both cases when combined with denoising.

4. DISCUSSION

By optimizing the user inputs for the EITs implemented in egs_cbct, the user is able to increase the scatter calculation efficiency by 4 orders of magnitude compared to running an analog simulation. It is however very important that a few potential pitfalls are avoided in the process.

The current implementation of delta transport is prone to user error. As shown for the clinical case, the use of an inappropriate medium can introduce a bias in the results. Care must thus be taken to ensure that the most attenuating medium in the simulation geometry is provided as the delta transport medium. When using a poly-energetic x-ray source, one must ensure that the delta transport medium is the most attenuating medium over the entire energy range. If no such medium can be defined from pre-existing media in the simulation geometry, one can circumvent the problem by adding another medium to the input file for the sole purpose of using it as the delta transport medium.

While the denoising algorithm provides the largest efficiency increase for any individual EIT in egs_cbct, it is not a true VRT and can introduce a bias in the simulation results. The user must ensure that the settings used are appropriate to remove statistical noise from the data without introducing a bias.

PDIS and RDIS require optimization of more than the two simple parameters in FS. Some of these additional parameters are correlated, making the optimization a complex task. The correlations might further cause fluctuations in the calculation efficiency, which makes it difficult to determine the optimal parameter values.

RDIS uses an array that is updated as the simulation progresses to optimize the splitting process, and a proper selection of the "learning phase" of this array must be made to ensure optimal efficiency. This also means that for the current implementation, the technique cannot retain the efficiency when being parallelized. It might however still be of interest to a user doing long and very accurate simulations. A similar issue is found for PDIS when combined with a so-called corrector, which has a similar adaptive behavior as RDIS. PDIS and RDIS are available in egs_cbct, but should be considered experimental splitting + RR techniques which require extensive testing before they can be employed at maximum efficiency.

While the present study is based on lengthy simulations, it is important to realize a few easy ways of reducing the required calculation time to obtain a desired level of statistical uncertainty faster. By studying the impact of reducing the resolution of the detector, phantom, and angular projections on the scatter estimation, further gains in efficiency can be achieved. For instance, if the pixel size of the high resolution detectors used in the present study are reduced by a factor of 2 on each side, so is the required calculation time to obtain the same level of uncertainty.

5. CONCLUSION

The present study demonstrates the need for geometry specific optimization of EIT parameters in egs_cbct to ensure the most efficient CBCT scatter calculations. It is recommended that forced detection is used at all times, and that delta transport is used with the proper delta transport medium input by the user. MFPTR may be beneficial for some geometries, with a modest efficiency increase found for one of two the geometries in this study. FS is simple to optimize, and provides around 50 times increase in efficiency. Proper use of the denoising algorithm provides the largest efficiency gain for any individual EIT in egs_cbct without introduction of a bias. In the present study, chi2max could be increased without compromising the simulation accuracy, while the increase of nmax and nmax2d did increase the MRE of the simulation result. Furthermore, the denoising algorithm requires the statistical uncertainty to be less than 30% before the algorithm is applied, to ensure the highest denoising efficiency.

When combined, the EITs in egs_cbct provided efficiency increases of more than 4 orders of magnitude in the present geometries compared to an analog simulation.

ACKNOWLEDGMENTS

R.S.T. is grateful for the hospitality of the Ionizing Radiation Standards Group at NRC where the majority of this work was completed during his visit. R.S.T. acknowledges Ph.D. funding from Elekta Ltd., Odense University Hospital and CIRRO—The Lundbeck Foundation Center for Interventional Research in Radiation Oncology and The Danish Council for Strategic Research.

[a]rune.slot.thing@rsyd.dk
[b]ernesto.mainegra-hing@nrc-cnrc.gc.ca

[1]J. Jarry, S. A. Graham, D. J. Moseley, D. J. Jaffray, J. H. Siewerdsen, and F. Verhaegen, "Characterization of scattered radiation in kV CBCT images using Monte Carlo simulations," Med. Phys. **33**, 4320–4329 (2006).
[2]G. Poludniowski, P. M. Evans, V. N. Hansen, and S. Webb, "An efficient Monte Carlo-based algorithm for scatter correction in keV cone-beam CT," Phys. Med. Biol. **54**, 3847–3864 (2009).
[3]G. J. Bootsma, F. Verhaegen, and D. A. Jaffray, "The effects of compensator and imaging geometry on the distribution of x-ray scatter in CBCT," Med. Phys. **38**, 897–914 (2011).
[4]G. J. Bootsma, F. Verhaegen, and D. A. Jaffray, "Spatial frequency spectrum of the x-ray scatter distribution in CBCT projections," Med. Phys. **40**, 111901 (15pp.) (2013).
[5]I. Kawrakow, "Accurate condensed history Monte Carlo simulation of electron transport. I. EGSnrc, the new EGS4 version," Med. Phys. **27**, 485–498 (2000).
[6]I. Kawrakow, E. Mainegra-Hing, D. W. O. Rogers, F. Tessier, and B. R. B. Walters, *The EGSnrc Code System: Monte Carlo Simulation of Electron and Photon Transport*, Technical Report PIRS–701 (5th printing) (National Research Council of Canada, Ottawa, Canada, 2009).
[7]E. Mainegra-Hing and I. Kawrakow, "Fast Monte Carlo calculation of scatter corrections for CBCT images," J. Phys.: Conf. Ser. **102**, 012017 (2008).
[8]E. Mainegra-Hing and I. Kawrakow, "Variance reduction techniques for fast Monte Carlo CBCT scatter correction calculations," Phys. Med. Biol. **55**, 4495–4507 (2010).
[9]J. Chang, L. Zhou, S. Wang, and K. S. Clifford Chao, "Panoramic cone beam computed tomography," Med. Phys. **39**, 2930–2946 (2012).
[10]P. Watson, E. Mainegra-Hing, E. Soisson, I. E. Naqa, and J. Seuntjens, "Implementation of a fast Monte Carlo scatter correction for cone-beam computed tomography," Med. Phys. **39**, 3625 (2012).
[11]P. Watson, E. Mainegra-Hing, E. Soisson, I. E. Naqa, and J. Seuntjens, "Scatter-B-Gon: Implementing a fast Monte Carlo cone-beam computed tomography scatter correction on real data," Med. Phys. **39**, 4644 (2012).
[12]R. S. Thing, U. Bernchou, E. Mainegra-Hing, and C. Brink, "Patient-specific scatter correction in clinical cone beam computed tomography imaging made possible by the combination of Monte Carlo simulations and a ray tracing algorithm," Acta Oncol. **52**, 1477–1483 (2013).
[13]M. Berger and J. Hubbell, *XCOM: Photon Cross Sections on a Personal Computer*, Technical Report NBSIR 87-3597 (NIST, Gaithersburg, MD, 1987).
[14]R. Kramer, H. J. Khoury, J. W. Vieira, and V. J. M. Lima, "MAX06 and FAX06: Update of two adult human phantoms for radiation protection dosimetry," Phys. Med. Biol. **51**, 3331–3346 (2006).
[15]P. Downes, R. Jarvis, E. Radu, I. Kawrakow, and E. Spezi, "Monte Carlo simulation and patient dosimetry for a kilovoltage cone-beam CT unit," Med. Phys. **36**, 4156–4167 (2009).
[16]E. Mainegra-Hing and I. Kawrakow, "Efficient x-ray tube simulations," Med. Phys. **33**, 2683–2690 (2006).
[17]I. Kawrakow, "On the de-noising of Monte Carlo calculated dose distributions," Phys. Med. Biol. **47**, 3087–3103 (2002).